Peer-reviewed version available at Sensors 2017, 17, 348; doi:doi:10.3390/s17020348

Article

An optoelectronic equivalent narrowband filter for high resolution optical spectrum analysis

Kunpeng Feng [1,†], Jiwen Cui [1,*,†], Hong Dang [1,†], Weidong Wu [1], Xun Sun [1], Xuelin Jiang [1,2] and Jiubin Tan [1]

[1] Center of Ultra-Precision Optoelectronic Instrument, Harbin Institute of Technology, Harbin 150080, China; aifenglin@gmail.com (K.F.); cuijiwen@hit.edu.cn (C. J.); sired_hit@163.com (H. D.); 543348876@qq.com (W. W.); 2503962673@qq.com (X. S.); jbtan@hit.edu.cn (J. T.)

[2] Shanghai Micro Electronics Equipment Co., Ltd., Shanghai 201203, China; jiangxuelin.hit@gmail.com (X. J.)

† These authors contributed equally to this work.

* Correspondence: cuijiwen@hit.edu.cn; Tel.: +86-451-86412896-417

Abstract: To achieve a narrow bandwidth optical filter with a wide swept range for new generation optical spectrum analysis (OSA) of high performance optical sensors, an optoelectronic equivalent narrowband filter (OENF) is investigated and a swept optical filter with bandwidth of several MHz and swept range of several ten nanometers is built using electric filters and a swept laser as local oscillator (LO). The principle of OENF is introduced and analysis of OENF system is presented. Two electric filters are optimized to be RBW filters for high and medium spectral resolution application. Both simulations and experiments are conducted to verify OENF principle and results show that power uncertainty is less than 1.2% and spectral resolution can reach 6 MHz. Then, a real-time wavelength calibration system consisting of HCN gas cell and Fabry–Pérot etalon is proposed to guarantee a wavelength accuracy of ±0.4 pm at C-band and to reduce the influence of phase noise and nonlinear velocity of swept LO. Finally, experiments on OSA of actual spectra of various optical sensors using OENF system are conducted. Experimental results indicate that OENF system has an excellent capacity in analysis of fine spectrum structures.

Keywords: optical spectrum analysis; optical sensors; optical filters; coherent optics

1. Introduction

Optical filters are essential in a wide range of applications, including optical communications [1], spectroscopy [2, 3], electronics [4] and optical sensors [5~9]. Especially, high resolution optical spectroscopy of high performance optical sensors has always attracted considerable interest and characters of optical spectrum analysis (OSA) such as resolution, dynamic range and measurable range highly depend on optical filters. With developments of high resolution OSA, demands of optical filters with a narrowband ranging from GHz to several MHz and a wide swept range upwards to several ten nanometers are rapidly increasing. However, these optical filters cannot be realized through common technologies.

To satisfy the requirement of new generation OSA of high performance optical sensors, much effort has been paid on investigation of swept narrowband optical filters. For example, fiber Bragg gratings (FBGs) inscribed in polymer optical fiber (POF) or POF devices have considerable losses and weak spectra [5~9]. Conventional optical filter technologies available include dispersion gratings, arrayed waveguide gratings, thin-film dielectric interference filters, Fabry–Pérot (FP) filters, and Mach–Zehnder interferometers (MZI). However, these devices have a difficulty providing both narrowband and wide swept range which resists the development of resolution and measurable range of OSA technology. Several methods have been proposed to implement desired optical filters. Resonance based optical filter photonic circuits integrated on silicon-on-insulator become an

Peer-reviewed version available at Sensors 2017, 17, 348; doi:doi:10.3390/s17020348

attractive technology because of miniaturization and easy tuning. Microring [10] and Sagnac loop within a ring resonator based optical filters [11] were proposed to build optical filters with bandwidth in GHz and swept range in several ten nanometers. Nevertheless, their bandwidth is proportion to swept range. That means the fineness is fixed and cannot be infinite. Then, researchers utilized nolinear optics principle including stimulated Brillouin scattering (SBS), stimulated Rayleigh scattering (SRS) and four-wave mixing (FWM) to construct optical filters [3, 4, 12]. Narrowband optical filters based on SBS in optical fibers were first proposed as a result of its highest gain in optical fibers. The gain spectrum bandwidth of SBS is several MHz and its gain spectrum can be swept with a tunable laser. This technique achieved a spectral resolution of 80 fm (~10 MHz) and a swept range of 40 nm in an 11.5-km length dispersion-shifted fiber [2]. Later, superposition of three Brillouin lines and vector attributes of SBS amplification in standard, weakly birefringence fibers, were utilized to improve its spectral resolution to 3 MHz [12]. To reduced bandwidth, FWM was investigated and Brillouin dynamic grating with a narrowband of 2.4 MHz was found in a 100-m length single-mode fiber (SMF) [13]. Subsequently, Yongkang Dong et al. optimized the SMF length to achieve an approximate birefringence-free SMF section between 0 m and 300 m and minimum spectral resolution as low as 0.5 MHz for optical spectrometry was demonstrated [3]. For SBS and FWM with SBS nolinear optics principle, the bandwidth of their optical filters cannot be further reduced because the intrinsic Brillouin bandwidth is several MHz-range. S. Preussler and T. Schneider combined SBS polarization pulling effect and heterodyne detection technique and achieved a resolution in the attometer or lower kilohertz range at 1550 nm [14]. Recently, Tao Zhu et al. used nonuniform fiber or trapped fiber to increase SBS threshold value 7 dB higher than that of the conventional SMF and the higher SBS gain spectrum was well suppressed [4, 15]. Thus, a SRS spectrum bandwidth of less than 10 kHz in 27-km length SMF was achieved and optical filters based on SRS were utilized in ultra-narrowband fiber laser. But how to realize a swept SRS filters for OSA technology is still an open issue. On the other hand, all optical filters based on nolinear optics principle should employ several hundred meters or even several ten kilometers SMF which makes them highly sensitive to environment, such as temperature drifts and vibrations. The weak nonlinear optics effects lead a low spectral gain or a weak refractive index modulation and the dynamic range of these technologies are not adequate.

In this paper, an optoelectronic equivalent narrowband filter (OENF) for high resolution OSA of high performance optical sensors is investigated and a swept optical filter with bandwidth of several MHz and swept range of several ten nanometers is built using electric filters and a swept laser as local oscillator (LO). OENF is based on coherent optics principle. The homodyne and heterodyne between signal under test (SUT) and LO is processed by an electric filter, thus only frequency components within the electric filter can achieve the following processes. The bandwidth of electric filters can be narrow and frequency components within the electric filter represent the optical power spectral density (OPSD) of SUT around the wavelength of LO. So a swept narrowband filter can be achieved when LO sweeps past SUT. The bandwidth of OENF can be adjusted through the design of electric filters and its swept range is determined by LO. This technology avoids using long SMF and overcomes the contradiction between narrowband and wide range.

This paper is organized as follows. Section 2 demonstrates OENF principle and establishes influence of OENF on OSA results. Section 3 describes experimental setup of OENF system and verifies its principle through experiments. Finally, conclusions are presented.

2. Principle

2.1 Principle of OENF

A schematic diagram of OENF system is illustrated in Figure 1 (a). The P polarized mode and S polarized mode of the SUT whose spectrum is ready to be characterized are splitted by polarizing beam splitter (PBS) to respectively perform OSA which is benefit of coherent optics principle of OENF. The P polarized modes of LO and SUT are combined in a polarization maintaining fiber (PMF) coupler to generate two wideband coherent optical signals. A balanced photodetector (BPD) is

utilized to receive coherent optical signals. Transimpedance amplifier (TZ) and blocking capacitor C within BPD extract heterodyne component and convert its photocurrent into composite alternating-current (AC) voltage signals. Composite AC voltage signals whose frequency is located in the narrowband resolution bandwidth (RBW) filter could pass RBW filter. Then signal directly characterizing OPSD of SUT at the wavelength of LO is obtained and subsequently measured using a power detector to get its root-mean-square (RMS). When swept LO sweeps at a linear rate, RMS describing OPSD of SUT at the wavelength of swept LO is continuously exported by power detector. Figure 1 (b) shows this process. RBW filter filtering wideband coherent signals can be equivalent to an OENF whose center is located at the wavelength of LO. The transfer function of RBW filter in frequency domain and envelop function of OENF in time domain keeps the same shape when LO linearly sweeps and the bandwidth of RBW filter is wide enough to contain a few ten periods of coherent signal [16, 17]. Figure 1 (b) also indicates LO wavelength and corresponding OENF of six points in time domain during sweep. Subsequently, the relationship between RMS or envelope and swept LO in time domain is achieved as shown at the bottom of Figure 1 (b). Then, RMS or envelope is smoothed by video bandwidth (VBW) filter and digitized. Finally, the spectrum of SUT is shown on the scope. For OSA of FBGs inscribed in polymer optical fiber and POF devices having considerable losses and weak spectra [5~9], OENF system has remarkable benefits compared with commercial OSA: (1) much more fine special structures of a broad FBG such as Chirped FBG in POF can be scoped which may be related to special sensing characters, manufacture inspection and other applications; (2) weak spectrum can be analyzed as a result that OENF system is based on coherent theory.

The signal process of OENF system has already been established in Ref. [16-20]. LO sweeps past SUT and forms chirp coherent signal in both frequency and time domain. The chirp coherent signal can be characterized as a linear-frequency-modulation chirp signal in time domain and transfer function of RBW filter in frequency domain can thus be transformed into a filter envelop function in time domain as an OENF for OSA. OENF has significant influence on OSA results.

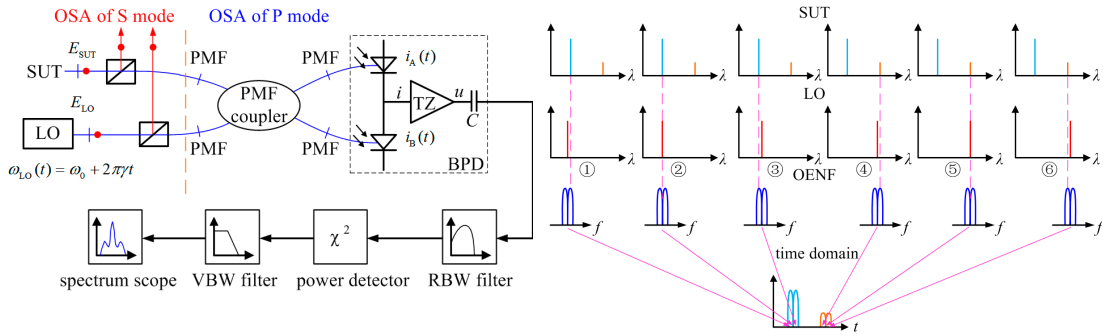

Figure 1. (a) Schematic diagram of OENF system. (b) Working process of OENF system.

2.2 Analysis of influence of OENF on OSA results

An arbitrary spectrum of SUT can be assumed as a combination of monochromatic components [21, 22]. OSA using OENF can be implemented through the analysis of every monochromatic signal. The monochromatic SUT is utilized to evaluate the influence of OENF on OSA results including power uncertainty and spectral resolution, and then SUT is extended to be an ensemble of complex monochromatic components to complete the analysis.

The coherent signal between monochromatic SUT and swept LO is processed by RBW filter and the output of RBW filter in time domain can be achieved. Then, a RMS power detector detects chirp signal within RBW filter and the signal representing its RMS power $\sqrt{\frac{1}{T}\int_0^T y^2(t)\,\mathrm{d}t}$ is continuously exported to form the time-domain RMS envelop of the amplitude product of swept OENF and

monochromatic SUT on the scope. The OPSD P_{SUT} of SUT is proportional to the integration of the square of RMS envelop function $S(t)$. Basing the Parseval's theorem, the OPSD P_{SUT} of SUT can be also written in a form of frequency domain as:

$$P_{SUT} = \frac{1}{2\pi}\int_{-\infty}^{+\infty}\left|\tilde{u}_{AC}(\omega)\right|^2\left|H(\omega)\right|^2 \mathrm{d}\omega = \int_0^t S^2(t)\mathrm{d}t \tag{1}$$

where, $\tilde{u}_{AC}(\omega)$ is frequency-domain signal of swept OENF, $H(\omega)$ is the transfer function of RBW filter and $S(t)$ is the time-domain RMS envelop function of swept OENF.

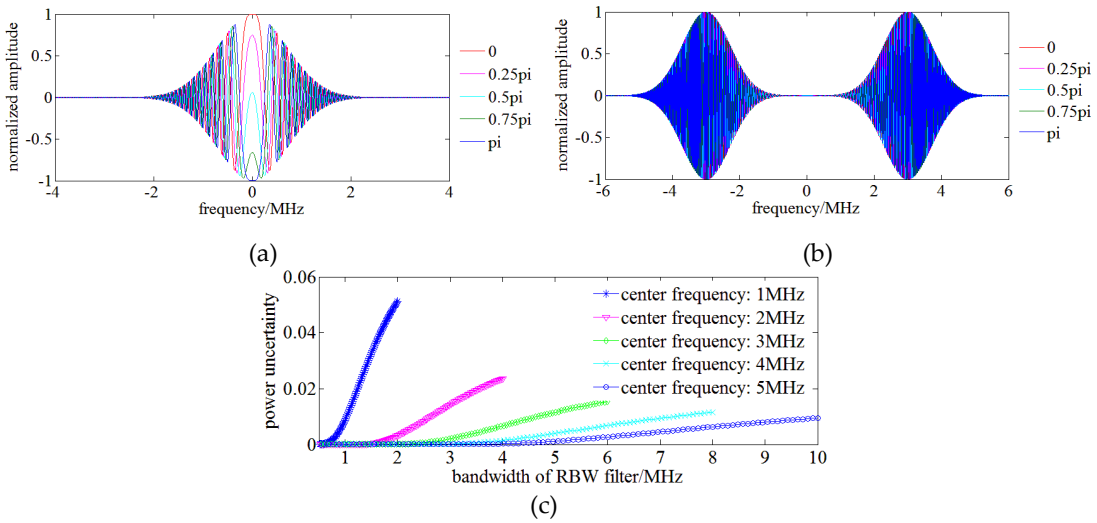

Figure 2. (a) Process of chirp signal with different initial phase using low pass RBW filter. (b) Process of chirp signal with different initial phase using band pass RBW filter. (c) The relationship between power uncertainty and parameters of RBW filter.

However, the coherent signal between monochromatic SUT and swept LO relates with their initial phase difference $\Delta\varphi$ which determines the chirp signal within RBW filter. A low pass Gauss filter with a bandwidth of 1 MHz and a band pass Gauss filter with a center frequency of 3 MHz and a bandwidth of 1 MHz is for example employed as RBW filter. The chirp signals within RBW filters in frequency domain are illustrated in Figure 2 (a) and (b). Basing on Eq. (1), Figure 2 (a) and (b) explicitly indicates that the phase difference $\Delta\varphi$ changes power of the frequency-domain chirp signal within the bandwidth or pass band of RBW filter and its influence on a low pass RBW filter is more significant.

The ratio of maximum OPSD error to minimum OPSD by varying the phase oscillating component of integrand kernel function represents the OPSD accuracy of SUT:

$$e_{P_{SUT}} = \frac{\max P_{SUT}(\Delta\varphi) - \min P_{SUT}(\Delta\varphi)}{\min P_{SUT}(\Delta\varphi)} \tag{2}$$

Figure 2 (c) shows the relationship between power uncertainty and parameters of a Gauss RBW filter. RBW filter allowing more low frequency components to pass are more easily influenced by phase difference $\Delta\varphi$ and has a much higher power uncertainty which agrees with the analysis based on Figure 2 (a) and (b). So a low pass RBW filter is not adopted for OSA and a narrow bandwidth and high center frequency RBW filter helps reduce the power fluctuation. On the other hand, the DC blocking capacitor of BPD also prevents low frequency components enter RBW filter and following processing modules.

The bandwidth and the center frequency of RBW filter also influence the spectral resolution of OENF for OSA. The bandwidth Δf of RBW filter is set to be 1 MHz and simulations are run by varying its center frequency f_0 from 2 MHz to 4 MHz. SUT consists of two monochromatic signals

1550 nm and 1550 nm+10 MHz. Swept LO starts at 1550 nm-7 MHz with a swept velocity 1 nm/s. Figure 3 shows the simulation result and it indicates that a sufficiently high center frequency leads to overlapping between double monochromatic signals which limits the spectral resolution. The spectral resolution of OENF for OSA can be an simply estimated as $2f_0 + \Delta f$. Considering the power uncertainty results of Figure 2 (c), a highest spectral resolution of 5 MHz with acceptable low power uncertainty of monochromatic SUT can be achieved with $f_0 = 2$ MHz and $\Delta f = 1$ MHz .

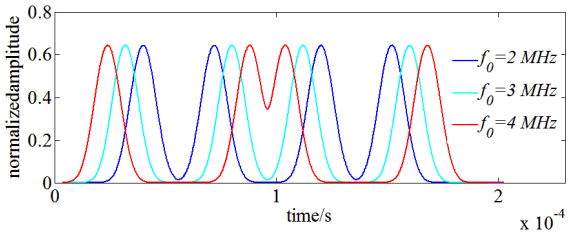

Figure 3. The relationship between overlapping of double monochromatic signals with the center frequency f_0 of RBW filter.

Once the parameters of RBW filter for highest spectral resolution are determined, the types of RBW filter become an issue. The engineering realizable filters have following types: Butterworth, Chebyshev, Gauss and Bessel. Butterworth, Chebyshev filter and Gauss is chosen as RBW filter but the Bessel filter is not considered due to its worst amplitude-frequency characteristics.

The absolute value of the transfer function of Butterworth filter can be expressed as:

$$H(\omega) = \frac{1}{\sqrt{1+\left(\frac{\omega-\omega_0}{\Delta\omega/2}\right)^{2n}}} \tag{3}$$

where, n is the order of the Butterworth filter, ω_0 is the center angular frequency of the filter and $\Delta\omega$ is the 3 dB bandwidth of the filter.

The absolute value of the transfer function of Chebyshev filter can be expressed as:

$$H(\omega) = \frac{1}{\sqrt{1+\xi^2 T_n^2\left(\frac{\omega-\omega_0}{\Delta\omega}\right)}} \tag{4}$$

where, ξ is the ripple factor, T_n is n^{th} order Chebyshev polynomial.

The absolute value of the transfer function of Gauss filter can be expressed as:

$$H(\omega) = \exp\left(-\ln\sqrt{2}\frac{(\omega-\omega_0)^2}{(\Delta\omega/2)^2}\right) \tag{5}$$

The influence of RBW filters of different types and orders on the power uncertainty of OSA results is investigated. Figure 4 (a) and (c) show the absolute value of the transfer function of Butterworth and Chebyshev filters of different orders. Simulations are run with these RBW filters of OENF for OSA and their power uncertainties are illustrated in Figure 4 (b) and (d). Simulations indicate that the power uncertainty of Butterworth filters initially decreases with the raise of order but rapidly increases when the order of Butterworth filters reaches 40th and power uncertainty gets its local minimum at medium bandwidth of RBW filter, which means that there is a power uncertainty balance between benefit of increase bandwidth and disbenefit of allowing low frequency components pass. On the other hand, the power uncertainty of Chebyshev filters directly increases with the raise of order. Both the Butterworth and Chebyshev filters of high orders are close to an ideal band pass filter as a rectangle shape in frequency domain decreasing the power uncertainty, which means a filter having character of smooth and fast attenuation could reduce the power uncertainty. Considering the physical realizability, a 10th order Butterworth and a 5th order Chebyshev filter are chosen for following analysis.

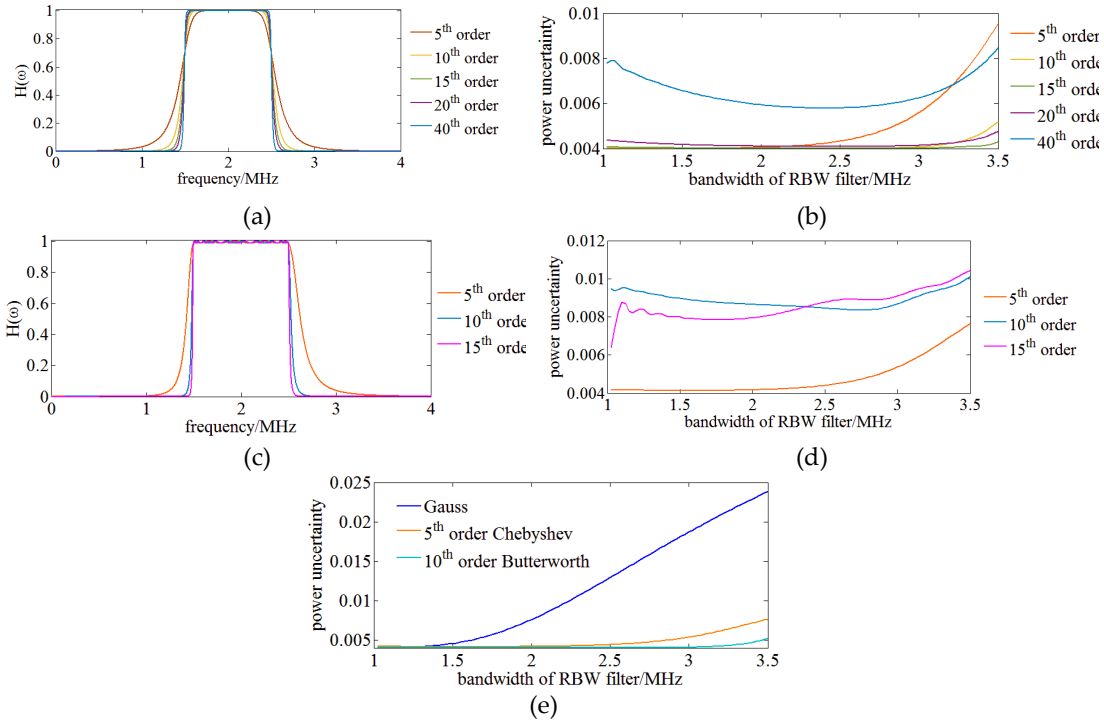

Figure 4. (a) The absolute value of the transfer function of Butterworth filters of different orders. (b) Power uncertainty of Butterworth filters of different orders as RBW filters. (c) The absolute value of the transfer function of Chebyshev filters of different orders. (d) Power uncertainty of Chebyshev filters of different orders as RBW filters. (e) Comparison of power uncertainty among Gauss, 5th order Chebyshev, 10th order Butterworth RBW filters.

Figure 4 (e) shows the relationship between power uncertainty and bandwidth of different RBW filters, 10th order Butterworth, 5th order Chebyshev filter and Gauss filter. It indicates that a 10th Butterworth achieves a minimum power uncertainty.

Besides power uncertainty, RBW filters of different types also have influence on the spectral resolution of OSA results. Simulation is run as following configurations: SUT is modeled as two adjacent monochromatic signals with a frequency difference of 5.5 MHz; three filters of 10th order Butterworth, 5th order Chebyshev filter and Gauss filter having a same center frequency of 2 MHz and bandwidth of 1 MHz are respectively employed as RBW filter of OENF. Figure 5 shows the time domain envelops of monochromatic SUT of three RBW filters. It indicates that Gauss filter has the largest overlapping between double monochromatic signals leading to the worst spectral resolution and Chebyshev filter has the biggest ripples in the pass band which has influence on power uncertainty. Therefore, the 10th order Butterworth filter is appropriately utilized as RBW in OENF system.

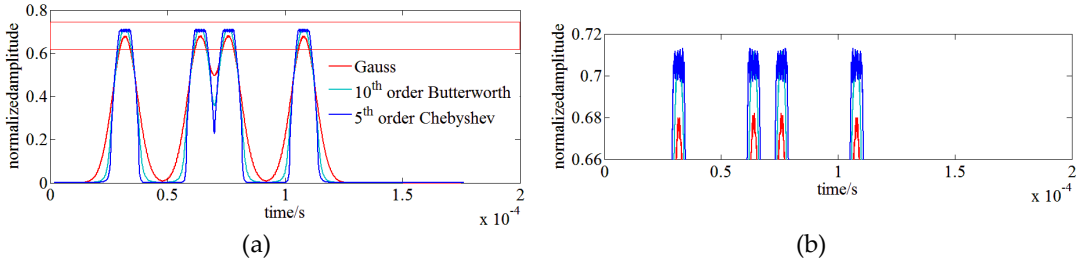

Figure 5. (a) Full view of the influence of RBW filters of different types on the spectral resolution. (b) Partial view of (a).

On the other hand, period number of chirp signal within RBW filter varies with swept velocity of swept LO which is also a factor leading power uncertainty. Actually, period number is inversely proportional to swept velocity. So chirp signal within RBW filter with a high swept velocity is sparse and more sensitive to the phase diversity. Figure 6 shows the relationship between power uncertainty and swept velocity with a 10th order Butterworth RBW filter of 2 MHz center frequency and 1 MHz bandwidth. A very short measurement time may be achieved by rising swept velocity of swept LO at the cost of power uncertainty.

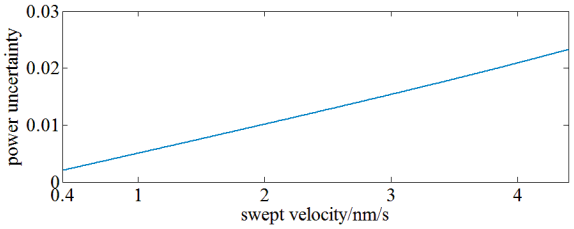

Figure 6. The relationship between power uncertainty and swept velocity of swept LO.

Finally, SUT is modeled as an ensemble of complex monochromatic components having a linewidth. The process of evaluating power uncertainty is similar to monochromatic SUT, but the power uncertainty terms of monochromatic signals experiences twice integration to obtain power uncertainty of complex monochromatic SUT. Figure 7 shows the power uncertainty of complex monochromatic SUT achieved with RBW filter of different center frequency and bandwidth. It indicates that a RBW filter with a higher center frequency could reduce the power uncertainty; a wider bandwidth of RBW filter could reduce the power uncertainty of a wide linewidth of SUT at the cost of spectral resolution. However, decrease of spectral resolution has no influence on OSA results of wider SUT with less fine spectrum structures. The power uncertainty decreases rapidly with the center frequency f_0 of RBW filter increasing from 2 MHz to 7.5 MHz, but change is slow down when the center frequency is higher than 7.5 MHz. On the other hand, the power uncertainty is further reduced through broadening the pass band Δf. So, two 10th order Butterworth filters of $f_0 = 7.5$ MHz, $\Delta f = 10$ MHz and $f_0 = 10$ MHz, $\Delta f = 10$ MHz are chosen as candidate RBW filter. Considering the spectral resolution, a 10th order Butterworth RBW filter of 7.5 MHz center frequency and 10 MHz bandwidth is finally utilized in 0.2 pm medium spectral resolution OENF system for OSA.

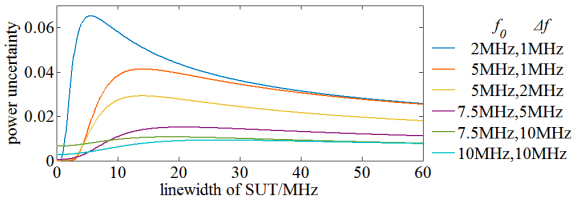

Figure 7. The power uncertainty of complex monochromatic SUT achieved with Butterworth RBW filter of different center frequency and bandwidth.

3. Experiments and discussion

3.1 Experimental setups

The experimental setup of OENF system is as same as the schematic diagram illustrated in Figure 1. The swept LO is an external cavity tunable (ECT) laser with a linewidth of 100 kHz and a fiber laser with a linewidth of 1 kHz. The all-fiber PBS and PMF coupler is made by AFR Company and the working axes are aligned to slow axes of PMF. The PDB is switchable gain and bandwidth PDB450C produced by Thorlabs with coverage of 800-1700 nm. An AC form of PDB450C is utilized and it has a common mode rejection ratio of over 30 dB. The power detector is made by AD8361 which is used for true power measurement and has a working bandwidth up to 2.5 GHZ with a high

Preprints (www.preprints.org) | NOT PEER-REVIEWED | Posted: 9 February 2017 doi:10.20944/preprints201702.0030.v1

Peer-reviewed version available at Sensors 2017, 17, 348; doi:doi:10.3390/s17020348

linear response. The integral time of AD8361 can be customized. RBW filters are designed using a software named FilterPro and the circuits are built by AD4817 with a high gain bandwidth product of 1 GHz which can ensure the actual transfer function is as least distortionless as possible. The VBW filters are also designed using FilterPro and their circuits are made of OP37 with a medium gain bandwidth product of 63 MHz. The analog signals are digitalized by PCI-1714 produced by ADVANTECH with a maximum sampling rate of 10 MHz. Software for acquiring and processing data from PCI-1714, and displaying SUT's spectrum is embedded on computer.

3.2 Verification of OENF's principle

In this section, results of simulation and experiment are compared to verify OENF's principle.

First, the influence of RBW filters type on the power uncertainty of OENF system for OSA is experimentally demonstrated. SUT is a fiber laser with a linewidth of 1 kHz. The wavelength of the fiber laser as SUT is 1550 nm and the swept LO is an ECT laser sweeping in the range of 1550±0.25 nm. Gauss, 5th order Chebyshev and 10th order Butterworth RBW filters with a center frequency of 2 MHz varies their bandwidth. These configurations are used to run the simulation and conduct experiments. The swept LO sweeps 30 times and the spectrum power is analyzed by OENF system. The maximum and minimum power is achieved and the power uncertainty is calculated using Eq. (2). Figure 8 (a) shows the comparison of power uncertainties by experiment with simulation results. It indicates that simulation results are consistent with the experimental data and errors may come from the noise and drift of the circuits. Error between simulation and experiment of 10th order Chebyshev filter is larger than the other filters which may be caused by ripples in its pass band. Figure 8 (a) also verifies that the 10th order Butterworth RBW filter has a minimum power uncertainty by experimental data.

Second, the influence of SUT's linewidth on the power uncertainty is verified. SUT of 1 kHz, 500 kHz, 2 MHz and 10 MHz and a swept fiber laser of 1 kHz as LO is utilized to conduct experiments and run simulations. A 10th order Butterworth filter with a center frequency of 2 MHz and a bandwidth of 1 MHz is employed as RBW filter. Their results are illustrated in Figure 8 (b) and have a similar trend but error rapidly increases with SUT's linewidth which may be caused by the phase noise and intensity noise of SUT of a wide linewidth.

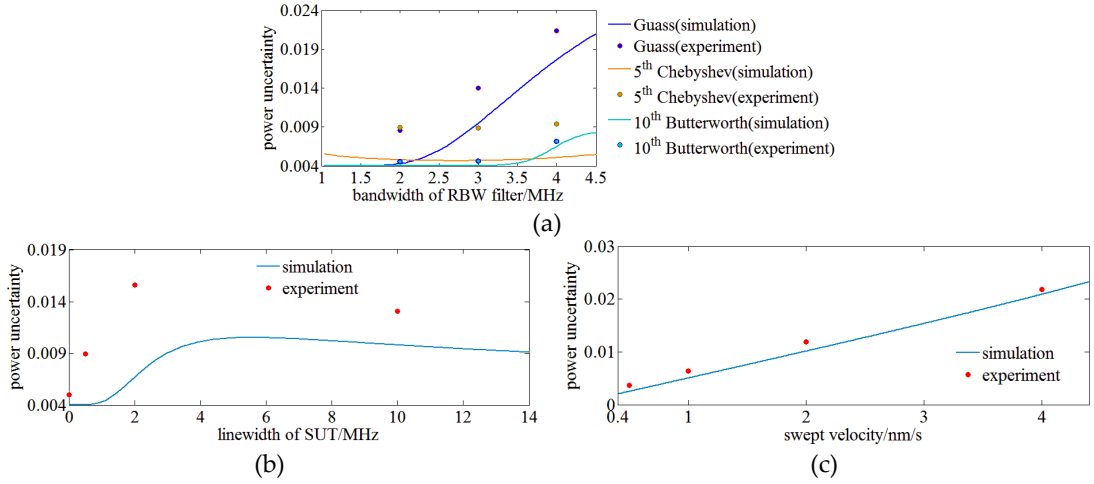

Figure 8. (a) Verification of RBW filter's type on power uncertainty of OENF system for OSA. (b) Verification of SUT's linewidth on power uncertainty of OENF system for OSA. (c) Verification of swept velocity of LO on power uncertainty of OENF system for OSA.

Third, the influence of swept velocity of LO on the power uncertainty is investigated. Basing on the analysis of section 2, swept velocity of swept LO changes the period number of chirp signal within the bandwidth of RBW filter and makes OENF system more sensitive to phase diversity. SUT of this experiment is a fiber laser with a linewidth of 1 kHz at 1550 nm and swept LO is an ECT laser sweeping in the range of 1550±0.25 nm. A 10th order Butterworth filter a center frequency of 2 MHz

Peer-reviewed version available at Sensors 2017, 17, 348; doi:doi:10.3390/s17020348

and of a bandwidth 1 MHz is employed as RBW filter. Figure 9 (a) shows the relationship between swept velocity and power uncertainty. It indicates that both simulation and experiment results agree with each other and the power uncertainty increases with the swept velocity.

Finally, the spectral resolution capacity is experimentally tested. An intensity modulated fiber laser of 1 kHz linewidth is employed as SUT for OSA. According to Jacobi-Anger identity, the fiber laser modulated by $LiNbO_3$ modulator has several peaks and their frequency interval is equal to the modulation frequency. The modulation signal is configured to achieve maximum 1st order peaks and zero 2nd order peaks. A 10th order Butterworth filter with a center frequency of 2 MHz and a bandwidth of 1 MHz is used as RBW filter and a 25 kHz low pass filter is used as VBW filter within the OENF system. Results of OENF is illustrated in Figure 9 and it indicates that a modulation signal of 6 MHz frequency interval (~48 fm in 1550 nm wavelength range) can be distinguished. So swept OENF can achieve a spectral resolution of 6 MHz. The experimental spectral resolution is slightly worse than designed value which may be caused by the difference between engineering realized and theoretically achieved RBW filter. During 6 MHz spectral resolution test, the resolution of OENF system reaches its limitation and the broader peak on the right may be caused by insufficient spectral resolution. The bandwidth of sidebands of the 9 MHz spectral resolution test is nearly equal. The frequency distance of both sidebands is not equal which is caused by nolinear swept velocity of LO. The wavelength calibration system could calibrate the swept velocity every 1 pm, however, the swept velocity within 1 pm is unknown and induces chirp.

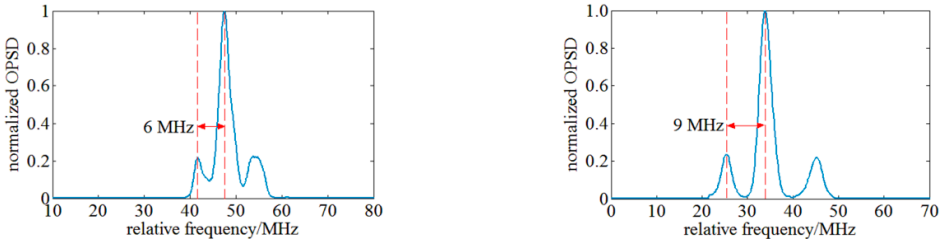

Figure 9. (a) OSA of 6 MHz frequency interval spectrum signal. (b) OSA of 9 MHz frequency interval spectrum signal.

3.3 Real-time wavelength calibration of swept LO

During the OSA, the LO sweeps the spectrum of SUT at a nominal velocity and the PCI-1714 acquires the analog signals with its inner clock at an equal time interval. However, the swept LO has phase noise and nonlinear velocity. These factors have deeply influences on the results of OSA, specifically, the spectrum shape. The wavelength of the swept LO should be calibrated in real time, so that the sampling points of data acquisition card (DAQ) can be connected with the wavelength.

The real-time wavelength calibration (RTWC) system is illustrated in Figure 10. The swept LO is dived into two parts at a ratio of 90:10, one part is for OSA and the other is for RTWC. Then the part of swept LO entering RTWC system is equally dived into three parts by a 1×3 fiber coupler, one part passes a hydrogen cyanide (HCN) gas cell for absolute wavelength calibration, one part passes a FP etalon, and another is directly detected by a photoelectricity conversion device for power normalization [23].

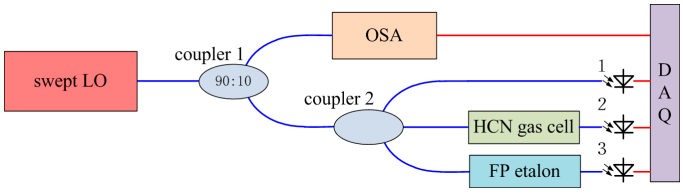

Figure 10. Schematic diagram of the RTWC system.

Preprints (www.preprints.org) | NOT PEER-REVIEWED | Posted: 9 February 2017 doi:10.20944/preprints201702.0030.v1

Peer-reviewed version available at Sensors 2017, 17, 348; doi:doi:10.3390/s17020348

The HCN gas cell has specific absorption lines covering from 1530 nm to 1560 nm at C-band. The HCN gas cell is made by Wavelength References and it is a NIST-traceable $H^{13}C^{14}N$ gas cell at 100 Torr (NIST SRMs 2519). The wavelength of specific absorption lines has an expanded uncertainty of less than ±0.2 pm. The FP etalon is made by Micron Optic and it has a nominal free spectral range (FSR) of 0.8 pm. The transmission peaks of FP etalon are very close in wavelength. It can be used to determine the real-time wavelength of the swept LO and sampling dates between two transmission peaks can be linearly interpolated to determine the real-time wavelength.

Figure 11 shows the signal processing of RTWC system. The signals of HCN gas cell and FP etalon is first normalized to suppress the power drift of LO. Then, the absorption lines of HCN gas cell is fitted using Voigt profile [24]. The pseudo-Voigt profile is utilized in this paper for approximation of the Voigt profile using a linear combination of a Gaussian curve and a Lorentzian curve instead of their convolution. The pseudo-Voigt profile can be written as:

$$V(\lambda) = \eta \exp\left[-\frac{4\ln 2(\lambda-\lambda_0)^2}{\gamma^2}\right] + (1-\eta)\frac{\gamma^2}{(\lambda-\lambda_0)^2+\gamma^2} \tag{6}$$

where, λ_0 is the center wavelength, γ is the bandwidth of a Gaussian curve and a Lorentzian curve, η is the ratio of Gaussian curve and a Lorentzian curve.

The initial wavelength of swept LO is roughly known which means that the initial wavelength is certainly located between two certain absorption lines. The absorption lines during swept period is determined once the direction of swept LO is known using Eq. (6). The up illustration of Figure 11(a) shows that the absorption lines are successively P4 (1545.23033(7) nm), P5 (1545.95549(7) nm), P6 (1546.69055(8) nm), P7 (1547.43558(24) nm), P8 (1548.19057(7) nm), P9 (1548.95555(4) nm) and P10 (1549.73051(4) nm). The center of FP etalon is located using centroid method and the bottom illustration of Figure 11 (a) shows location transmission peaks of FP etalon versus sampling time. Calculating the number of transmission peaks of FP etalon between two absorption lines of HCN gas cell, the average FSR of 0.7998 pm can be achieved. So the sampling points of DAQ can be connected with the wavelength in real-time and a wavelength accuracy of ±0.4 pm can be achieved during OSA.

Using this RTWC system and signal processing method, the swept velocity of LO at nominal velocity of 1 nm/s is calibrated as shown in Figure 11 (b). The swept velocity is about ±10 % around 1 nm/s. Therefore, the influence of phase noise and nonlinear velocity of swept LO can be effectively reduced in this way.

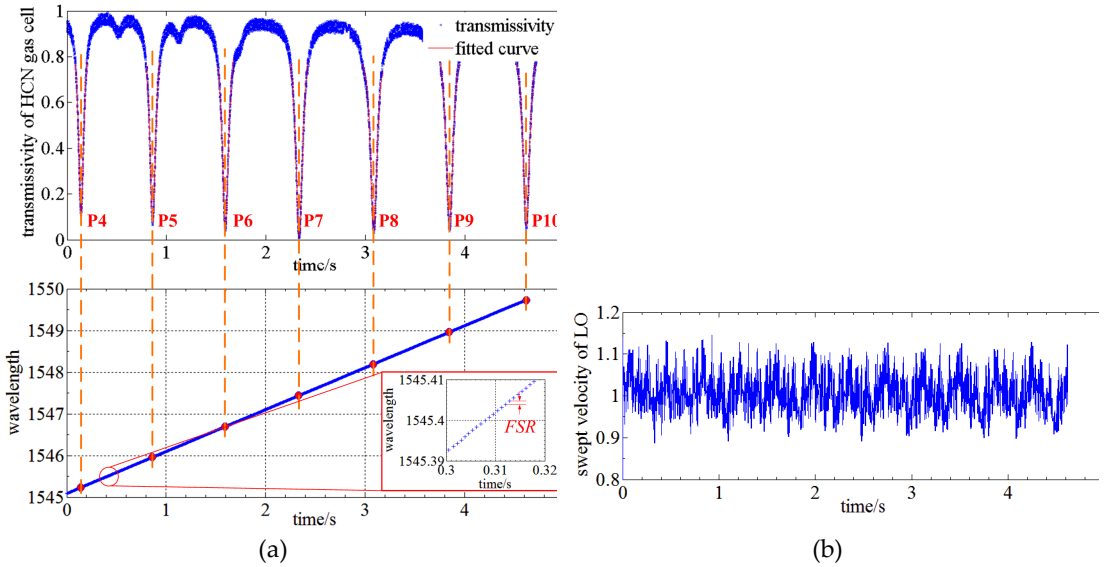

Figure 11. (a) Signal processing of RTWC system. (b) Swept velocity of LO at nominal velocity of 1nm/s.

3.4 OSA of fine spectrum structures of optical sensors using OENF system

In this section, optical spectra of optical sensors lighted by both wide amplified spontaneous emission (ASE) source and narrow laser source are measured using OENF system and these results are compared with results by Anritsu OSA of 30 pm spectral resolution.

First, ASE spectrum of phase-shift fiber Bragg grating (PS-FBG) sensor is measured. Spectrum of PS-FBG sensor is comparatively wide and the bandwidth can reach ~0.3 nm, however, it has a very narrow notch of ~1 pm in reflectance spectrum. A 10th order Butterworth filter with a center frequency of 7.5 MHz and a bandwidth of 10 MHz is as RBW filter and a 5 kHz low pass filter is as VBW filter of OENF system. The theoretical spectral resolution is 25 MHz (~0.2 pm in 1550 nm wavelength range). LO is an ECT laser.

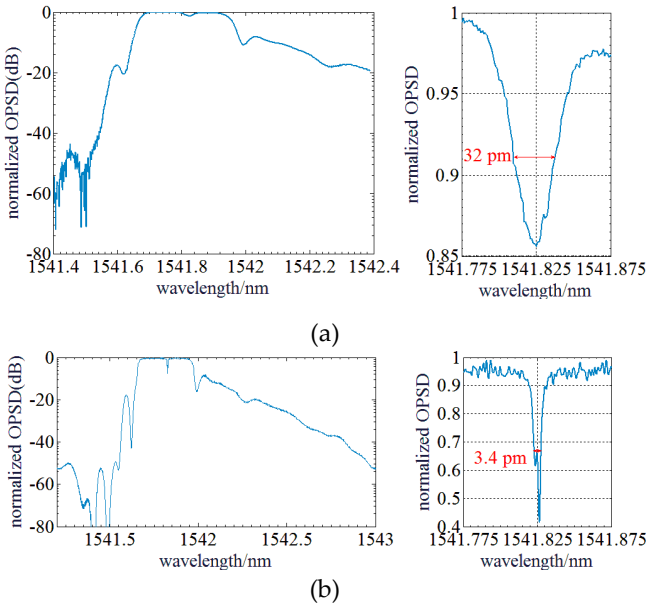

Figure 12. (a) Optical spectrum of PS-FBG sensor measured by Anritsu OSA. (b) Optical spectrum of PS-FBG sensor measured by OENF system.

Figure 12 shows the reflectance spectrum and spectral notch structure of PS-FBG sensor measured by both Anritsu OSA and OENF system. It indicates that reflectance spectrum profiles are same but the result by OENF system has some ripples which are probably caused by intensity noise of ASE source. However, the spectral notch structures of PS-FBG sensor measured are much different. OENF system gives a much narrow spectral notch which has more spectrum fine information and it is much close to the real spectrum. But the result by Anritsu OSA only provides a ~32 pm notch which is the actual spectral resolution of this OSA and fine information within the narrow notch is lost.

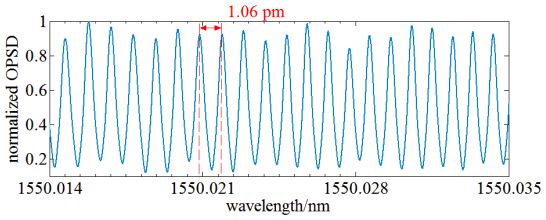

Figure 13. Optical spectrum of a fiber MZI sensor measured by OENF system.

Second, optical spectrum of a fiber MZI sensor is measured using OENF system. It has a sinusoidal spectrum with a norm spectral period of 1 pm±10%. An ASE source is served as input of fiber MZI sensor and a sinusoidal spectrum can be achieved using this fiber MZI sensor. A 10th order Butterworth filter with a center frequency of 7.5 MHz and a bandwidth of 10 MHz is as RBW filter

and a 5 kHz lowpass filter is as VBW filter of OENF system. LO is an ECT laser. Figure 13 shows the optical spectrum measured by OENF system. The optical spectrum has a sine shape and the optical spectral period is 1.06 pm within the uncertainty of the norm value of fiber MZI sensor.

Finally, optical spectrum of an optical frequency comb with a norm comb tooth spacing of 0.88 pm is tested by OENF system. A 10th order Butterworth filter with a center frequency of 2 MHz and a bandwidth of 1 MHz is as RBW filter and a 25 kHz lowpass filter is as VBW filter of OENF system. LO is an ECT laser. The result is illustrated in Figure 14. The achieved comb tooth spacing is 0.89 pm and linewidth of each comb is 13.9 MHz. The measurement error is less than 1.5%. Combs of an optical frequency comb inevitably have power diversity. So the measured OPSD diversity of each comb may come from the optical frequency comb source.

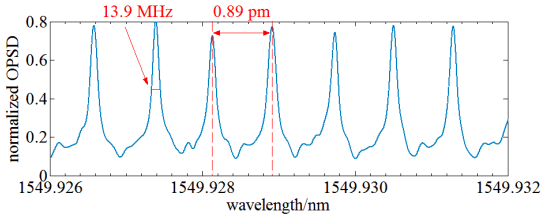

Figure 14. Optical spectrum of an optical frequency comb measured by OENF system.

4. Conclusions

In this paper, an OENF technology for OSA is theoretically and experimentally investigated. The principle of OENF is briefly introduced and much more effort is paid to analyze the influence of OENF on OSA. RBW filters are found to have significant influence on spectral resolution and power accuracy, two key parameters of OENF system. Considering the spectral resolution, RBW filter of 2 MHz center frequency and 1 MHz bandwidth can achieve an appropriate power uncertainty for monochromatic SUT. The power uncertainty can be further reduced by decreasing swept velocity. Subsequently, three types of engineering realizable RBW filter: Gauss, Chebyshev and Butterworth of different orders are respectively simulated to evaluate their power uncertainty and spectral resolution. A 10th order Butterworth RBW filter of 2 MHz center frequency and 1 MHz bandwidth has a smallest power uncertainty and a better spectral resolution than 5th order Chebyshev RBW filter. This 10th order Butterworth filter is thus chosen as RBW filter for high spectral resolution application. In a similar way, a 10th order Butterworth RBW filter of 7.5 MHz center frequency and 10 MHz bandwidth is employed as RBW for medium spectral resolution application. In order to reduce the influence of phase noise and nonlinear velocity of swept LO, a RTWC system consisting of HCN gas cell and FP etalon is proposed to achieve absolute and relative RTWC. With the help of RTWC system, the wavelength accuracy of OSA can be raised to ±0.4 pm at C-band and shape distortion of spectrum is reduced. Next, OENF principle is verified by experiments. Results show that experimental results on power uncertainty agree with that of simulation; the maximum power uncertainty is less than 2 %; a spectral resolution of 6 MHz can be achieved by OENF system. Finally, experiments on OSA of actual spectra including PS-FBG sensor, fiber MZI sensor and optical frequency comb using OENF system are conducted. Experimental results indicate that OENF system could achieve more spectrum fine information than that by commercial Anritsu OSA.

It can be concluded that OENF technology can simultaneously achieve a narrow bandwidth and a wide swept range. OENF system can also resist the drift and vibration and work in industrial site. These properties lead to a widely application in the fields of optical communication, spectroscopy, electronics, optical sensors and photography.

Acknowledgments: This work is funded by the National Natural Science Foundation of China (51575140).

Author Contributions: Kunpeng Feng and Xuelin Jiang theoretically analyzed the proposed OSA principle; Hong Dang, Weidong Wu and Xun Sun manufactured the hardware equipment, carried out several experiments and analyzed experimental data; Jiwen Cui and Jiubin Tan guided the study and put forward some valuable suggestions.

References

1. Trang Nguyen, Mohammad Arif Hossain, and Yeong Min Jang. Design and Implementation of a Novel Compatible Encoding Scheme in the Time Domain for Image Sensor Communication. *Sensors* **2016**, 16, 736.
2. Subias Domingo, J. M., Pelayo J., Villuendas F., Heras C. D., and Pellejer, E.. Very high resolution optical spectrometry by stimulated Brillouin scattering,. *IEEE Photonics Technol. Lett.* **2005**, 17, 855-857.
3. Yongkang Dong, Taofei Jiang, Lei Teng, Hongying Zhang, Liang Chen, Xiaoyi Bao, and Zhiwei Lu. Sub-MHz ultrahigh-resolution optical spectrometry based on Brillouin dynamic gratings. *Opt. Lett.* **2014**, 39, 2967-2970.
4. Thomas Chretiennot, David Dubuc, and Katia Grenier. Microwave-Based Microfluidic Sensor for Non-Destructive and Quantitative Glucose Monitoring in Aqueous Solution. *Sensors* **2016**, 16, 1733.
5. C. A. F. Marques, P. Antunes, P. Mergo, D. J. Webb, and P. André. Chirped Bragg gratings in PMMA step-index polymer optical fiber. *IEEE Photonics Technol. Lett.* **2017**, in pressed.
6. Jiwen Cui, Kunpeng Feng, Yang Hu, Junying Li, Hong Dang, and Jiubin Tan. Double fiber probe with a single fiber Bragg grating based on the capillary-driven self-assembly fabrication method for dimensional measurement of micro parts. *Opt. Express* **2015**, 23, 32926-32940.
7. Xuehao Hu, David Saez-Rodriguez, Carlos Marques, Ole Bang, David J Webb, Patrice Mégret, and Christophe Caucheteur. Polarization effects in polymer FBGs: study and use for transverse force sensing. *Opt. Express* **2015**, 23, 4581-4590.
8. Carlos A. F. Marques, Gang-Ding Peng, and David J. Webb. Highly sensitive liquid level monitoring system utilizing polymer fiber Bragg gratings. *Opt. Express* **2015**, 23, 6058-6072.
9. Ricardo Oliveira, Lúcia Bilro, and Rogério Nogueira. Bragg gratings in a few mode microstructured polymer optical fiber in less than 30 seconds. *Opt. Express* **2015**, 23, 10181-10187.
10. Romain Guider, Davide Gandolfi, Tatevik Chalyan, Laura Pasquardini, Alina Samusenko, Georg Pucker, Cecilia Pederzolli, and Lorenzo Pavesi. Design and Optimization of SiON Ring Resonator-Based Biosensors for Aflatoxin M1 Detection. *Sensors* **2015**, 15, 17300-17312.
11. Hyunjin Kim, Umesh Sampath, and Minho Song. Multi-Stress Monitoring System with Fiber-Optic Mandrels and Fiber Bragg Grating Sensors in a Sagnac Loop. *Sensors* **2015**, 15, 18579-18586.
12. Stefan Preussler, Avi Zadok, Andrzej Wiatrek, Moshe Tur, and Thomas Schneider. Enhancement of spectral resolution and optical rejection ratio of Brillouin optical spectral analysis using polarization pulling. *Opt. Express* **2012**, 20, 14734-14745.
13. Song K. Y.. Operation of Brillouin dynamic grating in single-mode optical fibers. *Opt. Lett.* **2011**, 36, 4686-4688.
14. S. Preussler and T. Schneider. Attometer resolution spectral analysis based on polarization pulling assisted Brillouin scattering merged with heterodyne detection. *Opt. Express* **2015**, 23, 26879-26887.
15. Tao Zhu, Xiaoyi Bao, Liang Chen, Hao Liang, and Yongkang Dong. Experimental study on stimulated Rayleigh scattering in optical fibers. *Opt. Express* **2010**, 18, 22958-22963.
16. Bogdan Szafraniec, Anthony Lee, Joanne Y. Law, William Ian McAlexander, Richard D. Pering, Tun S. Tan, and Douglas M. Baney. Swept Coherent Optical Spectrum Analysis. IEEE *Trans. Instrum. Meas.* **2004**, 53, 203-215.
17. Baney D. M., Szafraniec B., and Motamedi A.. Coherent optical spectrum analyzer. *IEEE Photonics Technol. Lett.* **2002**, 14, 355-357.
18. Szafraniec B., Lee A., Law J. Y., McAlexander W. I., Pering R. D., Tan T. S., and Baney D. M.. Swept coherent optical spectrum analysis. *IEEE Trans. Instrum. Meas*. **2004**, 53, 203-215.
19. M. O. van Deventer, C. M. de Blok, and C. Park. High-dynamic-range heterodyne measurement of optical spectra. *Opt. Lett.* **1991**, 16, 678-680.
20. T. Kataoka and K. Hagimoto. High resolution optical spectrum analyzer using a heterodyne detection technique. *IEEE Instrumentation and Measurement Technology Conference* 1994, 1, 234–237.
21. Kunpeng Feng, Jiwen Cui, Hong Dang, Shiyuan Zhao, Weidong Wu, Jiubin Tan. Investigation and development of a high spectral resolution coherent optical spectrum analysis system. *Opt. Express* **2016**, 24, 25389-25402.
22. Ning Hua Zhu, Wei Li, Jian Hong Ke, Hong Guang Zhang, Jiang Wei Man, and Jian Guo Liu. Optoelectronic devices and properties. Optical spectral structure and frequency coherence, **2011**, 27, Oleg Sergiyenko, Ed. Rijeka: InTech, pp. 603-628.

23. E Rivera and D J Thomson. Accurate strain measurements with fiber Bragg sensors and wavelength references. *Smart Mater. Struct.* **2006**, 15, 325-330.
24. Sarah L. Gilbert, William C. Swann, Chih-Ming Wang. Hydrogen Cyanide $H^{13}C^{14}N$ Absorption Reference for 1530 nm to 1565 nm Wavelength Calibration – SRM 2519a. *NIST special publication* **2005**, 260, 137.